Uniformity and Crosstalk in Multi-Anode Photomultiplier Tubes

A thesis submitted in partial fulfillment of the requirements for the degree of Bachelor of Science degree in Physics from the College of William and Mary

by

Oscar J Deaver

Advisor: Wouter Deconinck

Senior Research Coordinator: Gina Hoatson

Date: April 17, 2015

Uniformity and Crosstalk in Multi-anode Photomultiplier Tubes

Oscar Deaver

April 17, 2015

1 Abstract

Multi-anode photomultiplier tubes can process signals from 64 different sources, by splitting the anode into 64 different segments, and analyzing the signal from each of those segments separately. With a precise understanding of how they function, they can therefore be used as a substitute for 64 or 16 separate single photomultiplier tubes (PMTs). This could increase the convenience and reduce the cost of many larger experiments, which require large scintillating arrays, and therefore many PMTs in order to obtain better precision. However we need to have both a measure of how much variance in signal gain there is between different anodes, and how much cross-talk there is between adjacent channels. In order to measure the uniformity we compared signal strength from a fiber optic of uniform intensity, when placed at the center of each anode. In order to measure crosstalk we looked at the signal strength in the adjacent anodes when the LED was at the center of an anode. Our uniformity measurements showed that all the anodes were within the factory allowance, and showed that uniformity is consistent across several voltages below 1000V. This data will allow experiments to run at lower gains, thereby increasing the lifetime of the PMT. Our measure of the signal strength of the crosstalk will allow later experiments to take it's effect into account.

2 Introduction

One of the detectors in the Solenoidal Large Intensity Device (SoLID) in Hall A at Jefferson Lab is a large calorimeter, which will require large arrays of scintillators. These scintillators, when struck by particles, emit small flashes of light, which are

carried through fiber optics to a Photomultiplier tube (PMT). These change this small amount of light into an electrical signal large enough to read. A basic PMT design is shown in Figure 1. A series of dynodes, and on one end a photocathode, are kept at progressively higher voltages than the anode. When struck by a photon, the photocathode emits an electron, which is accelerated by the lower voltage towards the first dynode. When it strikes the dynode it emits multiple electrons, which are then accelerated towards the next dynode. This process of exponential growth of the number of electrons, known as an electron avalanche, leads to the anode receiving a measurable large current by the time the signal reaches it.

The Multi-anode PMT (MaPMT) has a similar design to that shown in Figure 2. 64 anodes are placed in a square array (in the ones being tested, 4 by 4 and 8 by 8), and dynodes are layered in a venetian blinds pattern above them, each layer being a progressively higher voltage. A single photocathode layer is placed above them. There are two issues with this design. The first is that we cannot individually optimize each of the anodes, since the high voltage is uniform across the MaPMT. The second is that there is no way to totally prevent electrons from one anode?s avalanche from falling on adjacent anodes, since they are packed so tightly. This is called crosstalk. The purposes of our tests then, were to get a precise measure of the gain of each anode, and to measure, or at least put an upper bound on the level of this crosstalk.

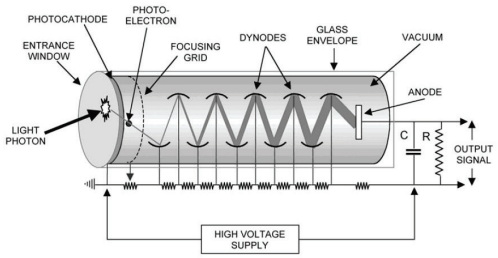

Figure 1: A basic design of a PMT.

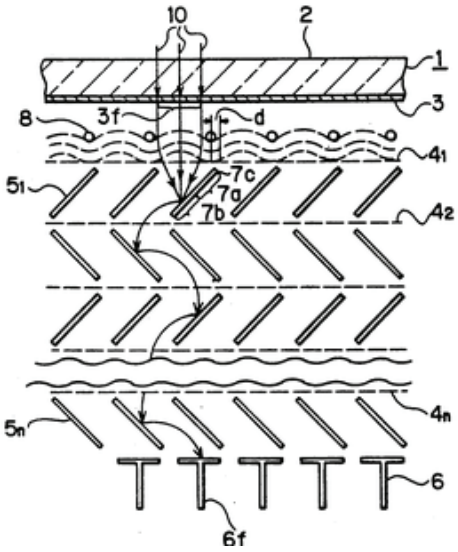

Figure 2: The MaPMT cross section. A single photocathode layer is above rows of dynodes and anodes.

3 Materials and Methods

As said above, Hamamatsu's 64-anode MaPMT consists of an array of 8 by 8 anodes, with 12 layers of dynodes above them in a venetian blinds pattern and a photocathode covering the whole thing. The dimensions of the anodes are given in Figure 3, which also shows how the pixels are numbered. The 16-anode MaPMT consists of a 4 by 4 array, again with 12 layers of dynodes in a venetian blinds

pattern beneath a photocathode layer. The dimensions are given in figure 4. Each anode is a $4.3mm$ square.

Signals to the MaPMTs were delivered via the end a fiber optic of a diameter of about 1mm. At the opposite end of the legnth of the fiber optic is an LED which delivers signals of variable intensity. The end of the fiber optic pointed at the MaPMT is moved from above one anode to above another via a 2-d mobile table, driven by two step motors. Both of these step motors were calibrated at minimum at the start of every day, and at the start of every full sweep of all the anodes, when measurements were taken to within 10nm per step. As the number of steps per pixel was never greater than 4000, this corresponds to a maximum .04mm error across one pixel, or $.04mm \times 8 \times \sqrt{2} = 0.45mm$ maximum error from corner to corner.

An electronic diagram of the the entire apparatus used can be seen in figure 7. In addition to what is pictured, a level translator was used at several points in order to change the signal to the necessary form for the modules being used.

In order to process the output of the MaPMT, a charge-to-digital converter (QDC) was used. It has 16 channels, and can handle the output from two columns of anodes at a time. The charge-to-signal ratio for each channel was precisely calibrated by sending signals of known magnitude through the channel and looking at the output (to be redone). Four signals of different magnitude were sent through the QDC channel, and the output mean and variance were recorded. The slope of the line fit to the resulting Current vs. Signal graph was used as the charge-to-signal ratio for that channel. An example fit is shown in Figure 5.

Measurements were taken by placing the end of the fiber optic no further than 1mm away from the surface of the MaPMT. An LED sent light into one end of the

fiber, and the LED was turned on and off at a rate of 1kH. The data acquisition system (DAQ) alternated taking measurements when it was on, to find the signal strength, and when it was off, to give us a resting signal to compare it to, called the pedestal. A sample measurement is shown in Figure 6. The signal strength was measured as the difference between the signal peak and the pedestal peak, scaled according to the QDC calibrations above based on the channel used.

Measuring the gain of each anode required a measure of how position sensitive the gain would be, in the direction parallel to the surface of the photocathode (the x-y direction). From above we know the spacial uncertainties in the position of our fiber optic as it moves across the MaPMT.

The fiber optic was moved at intervals of .8mm across the center of an anode. The results are shown in Figure 9. There is a circle of radius .8mm where the gain does not change by more than 3.5%. From the considerations above, it is reasonably certain that as the maximum change of the fiber's position could be $.45mm$, we can conclude that the fiber was within that circle for the measurements taken.

Finally, a test must be conducted to see how gain changes with distance from the photocathode (z direction). This will be taken over a range of about 1mm. The uncertainty in placement of the end of the fiber optic is $.5mm$.

By examining the signals from the adjacent anodes during these fine-spatial movement tests, we can also place error bounds on our crosstalk measurements. For sample pixels vertically, horizontally, and diagonally adjacent to the target pixel, I took measurements of signal strength across vertical and horizontal movement. An example of such a measurment can be found in figure 10. To get total uncertainty in the $x - y$ direction, I considered the measurement at .85mm off of

center for both directions, then took the bigger one as Δx and Δy. Then the total is $\sigma_{sys} = \sqrt{\Delta x^2 + \Delta y^2}$.

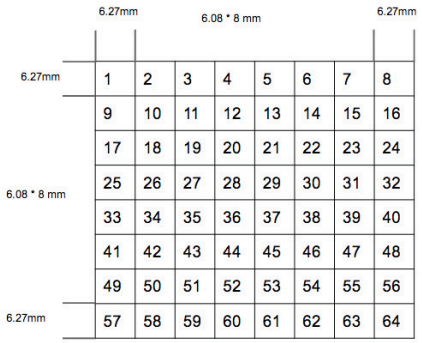

Figure 3: Shows the dimensions of each anode of the 64-anode PMT, as well as the numbering scheme.

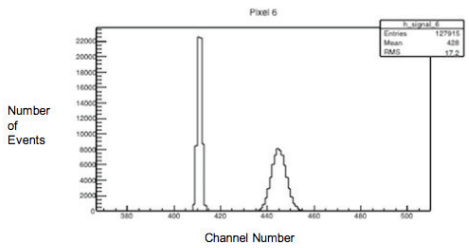

Figure 4: Example pedestal and signal peaks from a single run. Means and RMSs for both were found by fitting a Gaussian curve to both peaks.

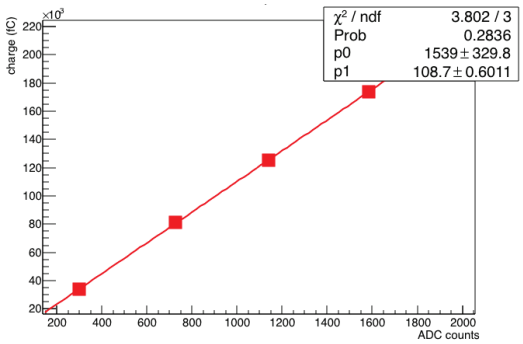

Figure 5: The charge/count ratio of channel 18. Fit is of the form $y = p1x + p0$. Errors on individual measurements are inside the red dots.

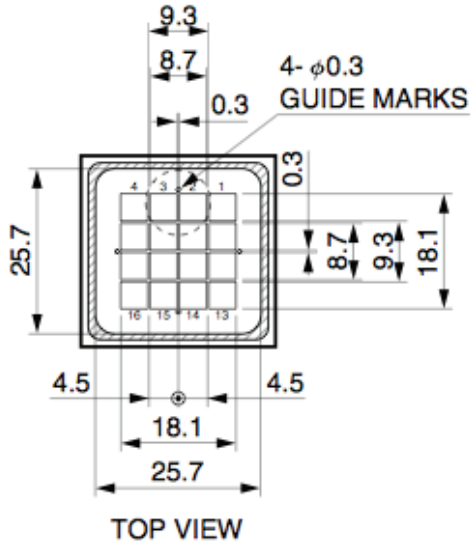

Figure 6: Shows the dimensions of each anode of the 16-anode PMT

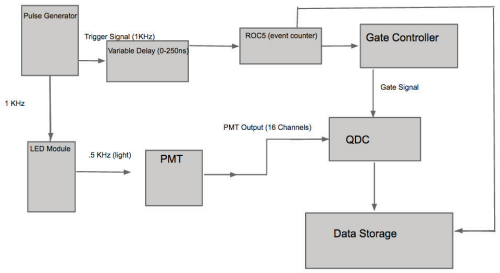

Figure 7: Shows the overall signal route in the experimental setup.

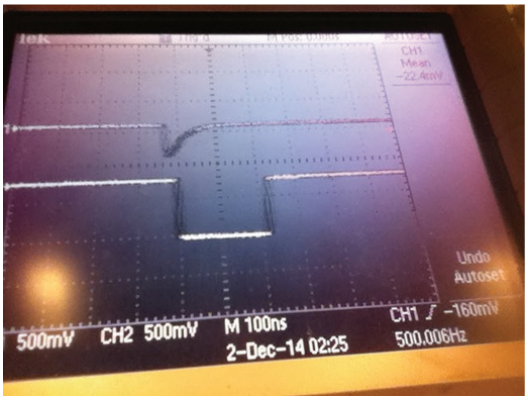

Figure 8: Shows the PMT output alongside the gate signal.

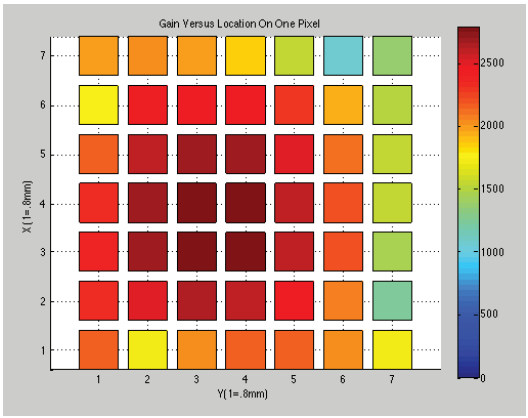

Figure 9: The gain versus position of fiber in one anode. Gain given in channel numbers between pedestal and signal.

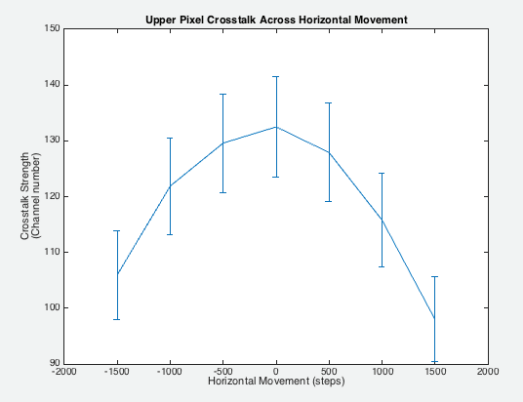

Figure 10: A sample of gain in vertically adjacent pixels over fine movement, this time in the x-direction. Δx was taken to be whichever one of the measurements 500 steps off was further from the center, in this case the +500 measurement.

In taking the uniformity measurements, we simply placed the fiber at the center of each anode and took measurements as above, across all 64 anodes. Measurements were taken at voltages of 450V, 500V, and 1000V. Crosstalk measurements were taken at anodes 11, 14, 43, and 46, at voltages of 500V and 850V. For each pixel and voltage pair, we took measurements from the anode which the fiber optic was centered on and the 8 adjacent ones. Since this involves three separate columns, two separate runs were required in order to obtain the data from all three columns.

4 Issues

Between the taking of the data for the 64-anode PMT and now, I've run into a number of issues with the data acquisition system and the general setup of the experiment. Much of the intervening time was spent both fixing these problems, and familiarizing myself with the data acquisition system enough to troubleshoot

basic issues by myself.

One issue initially was that, referring to figure 7, the noise on the line into the event counter was too high, leading to the DAQ registering many false events. This was solved by placing a discriminator along that line.

Note that this setup in figure 7 requires the signal from the PMT to arrive at the same time as the gate signal. This can be seen in figure 8, where the PMT output is on the top and the gate signal on the bottom. Since the QDC acquires a measurement by integrating the PMT signal over the interval determined by the gate, the delay on the gate signal must be adjusted so that the entire signal peak falls within the gate. As the variable delay source was finicky, this had to be frequently readjusted. One of the major problems I faced this year is shown in that picture, that the gate signal lagged the PMT signal even at 0 delay from the variable delay source, ever since the discriminator was placed in that line. I've prepared to introduce another delay source between the pulse generator and the LED module in an attempt to slow the PMT signal.

In my first attempt to do so, I first cut the cable between the pulse generator and the LED board, then placed a level translator in between, to make sure the connection was solid prior to adding the variable delay module. However, both the LED and pulser modules were made to handle signal of a different logic language than the TTL input and output I used, and so fuses on both were blown. Figuring out that that was what happened took considerable time.

5 Results

The results for our uniformity measurements are shown in Tables 1-3 for voltages 450V, 500V, and 1000V, respectively. Figures 11 and 12 show uniformity at 1000V compared to that given by the MaPMT's factory specifications. Statistical uncertainty was derived from the RMS's of the signal and pedestal peaks (δ_s and δ_p, respectively), using the formula $\delta = \sqrt{\delta_s^2 + \delta_p^2}$.

$38.4 \pm 1.3(\pm 1.0)$	$38.0 \pm 1.3(\pm 1.1)$	$36.2 \pm 1.3(\pm 1.0)$	$42.1 \pm 1.5(\pm 1.1)$	$43.7 \pm 1.5(\pm 1.1)$	$41.6 \pm 1.5(\pm 1.1)$	$43.1 \pm 1.5(\pm 1.1)$	$38.1 \pm 1.3(\pm 1.1)$
$40.2 \pm 1.5(\pm 1.1)$	$40.3 \pm 1.4(\pm 1.1)$	$36.0 \pm 1.3(\pm 1.1)$	$39.0 \pm 1.4(\pm 1.1)$	$37.1 \pm 1.3(\pm 1.1)$	$39.6 \pm 1.4(\pm 1.1)$	$44.9 \pm 1.6(\pm 1.1)$	$41.5 \pm 1.5(\pm 1.1)$
$41.7 \pm 1.5(\pm 1.1)$	$40.2 \pm 1.4(\pm 1.1)$	$39.1 \pm 1.4(\pm 1.1)$	$39.3 \pm 1.4(\pm 1.1)$	$38.5 \pm 1.3 \pm 1.1)$	$37.8 \pm 1.3(\pm 1.1)$	$43.3 \pm 1.5(\pm 1.1)$	$42.2 \pm 1.5(\pm 1.2)$
$42.2 \pm 1.5(\pm 1.1)$	$40.7 \pm 1.4(\pm 1.3)$	$41.4 \pm 1.5(\pm 1.1)$	$42.0 \pm 1.5(\pm 1.3)$	$42.5 \pm 1.5(\pm 1.1)$	$38.0 \pm 1.3(\pm 1.3)$	$44.3 \pm 1.6(\pm 1.1)$	$42.5 \pm 1.5(\pm 1.3)$
$41.7 \pm 1.5(\pm 1.1)$	$41.2 \pm 1.4(\pm 1.3)$	$41.5 \pm 1.5(\pm 1.1)$	$43.3 \pm 1.5(\pm 1.3)$	$43.2 \pm 1.5(\pm 1.1)$	$39.1 \pm 1.4(\pm 1.3)$	$43.4 \pm 1.5(\pm 1.1)$	$42.7 \pm 1.5(\pm 1.3)$
$42.5 \pm 1.5(\pm 1.1)$	$42.4 \pm 1.5(\pm 1.2)$	$40.2 \pm 1.4(\pm 1.1)$	$41.5 \pm 1.5(\pm 1.2)$	$41.0 \pm 1.4(\pm 1.1)$	$38.1 \pm 1.3(\pm 1.2)$	$43.7 \pm 1.5(\pm 1.1)$	$41.8 \pm 1.5(\pm 1.1)$
$43.8 \pm 1.5(\pm 1.1)$	$42.4 \pm 1.5(\pm 1.2)$	$43.1 \pm 1.5(\pm 1.1)$	$42.3 \pm 1.5(\pm 1.3)$	$42.9 \pm 1.5(\pm 1.1)$	$34.1 \pm 1.2(\pm 1.3)$	$45.1 \pm 1.6(\pm 1.1)$	$37.5 \pm 1.3(\pm 1.2)$
$43.8 \pm 1.5(\pm 1.1)$	$45.0 \pm 1.6(\pm 1.1)$	$45.1 \pm 1.6(\pm 1.1)$	$48.2 \pm 1.7(\pm 1.2)$	$46.0 \pm 1.6(\pm 1.1)$	$41.8 \pm 1.5(\pm 1.2)$	$43.7 \pm 1.5(\pm 1.1)$	$36.5 \pm 1.3(\pm 1.1)$

Table 1: Uniformity measurements at 450V, arranged according to Figure 3. Systematic (statistical) uncertainties are listed. Numbers are in channels between the signal and pedestal peaks.

$70.6 \pm 2.5(\pm 1.6)$	$79.2 \pm 2.8(\pm 1.7)$	$84.3 \pm 3.0(\pm 1.6)$	$90.3 \pm 3.2(\pm 1.6)$	$96.7 \pm 3.4(\pm 1.6)$	$97.2 \pm 3.4(\pm 1.8)$	$88.5 \pm 3.1(\pm 1.5)$	$81.8 \pm 2.9(\pm 1.7)$
$79.0 \pm 2.8(\pm 1.5)$	$82.6 \pm 2.9(\pm 1.6)$	$84.9 \pm 3.0(\pm 1.5)$	$85.7 \pm 3.0(\pm 1.6)$	$84.3 \pm 3.0(\pm 1.5)$	$94.3 \pm 3.3(\pm 1.6)$	$94.3 \pm 3.3(\pm 1.5)$	$86 \pm 3(\pm 1.6)$
$76.8 \pm 2.7(\pm 1.6)$	$78.1 \pm 2.7(\pm 1.8)$	$83.2 \pm 2.9(\pm 1.6)$	$82.0 \pm 2.9(\pm 1.7)$	$81.1 \pm 2.8(\pm 1.6)$	$86.5 \pm 3.0(\pm 1.7)$	$89.4 \pm 3.1(\pm 1.6)$	$87.2 \pm 3.1(\pm 1.7)$
$77.3 \pm 2.7(\pm 1.6)$	$75.4 \pm 2.6(\pm 2.1)$	$86.9 \pm 3.0(\pm 1.8)$	$85.7 \pm 3.0(\pm 2.1)$	$87.6 \pm 3.1(\pm 1.8)$	$84.8 \pm 3.0(\pm 2.1)$	$89.8 \pm 3.1(\pm 1.7)$	$87.5 \pm 3.1(\pm 2.1)$
$77.5 \pm 2.7(\pm 1.7)$	$75.5 \pm 2.6(\pm 2.2)$	$85.5 \pm 3.0(\pm 1.8)$	$89.6 \pm 3.1(\pm 1.9)$	$90.4 \pm 3.2(\pm 1.8)$	$87.4 \pm 3.1(\pm 2.3)$	$88.3 \pm 3.1(\pm 1.7)$	$88.9 \pm 3.1(\pm 2.2)$
$78.3 \pm 2.7(\pm 1.6)$	$77.3 \pm 2.7(\pm 1.7)$	$83.2 \pm 2.9(\pm 1.7)$	$84.6 \pm 3.0(\pm 1.8)$	$86.2 \pm 3.0(\pm 1.8)$	$87.6 \pm 3.1(\pm 1.8)$	$90.4 \pm 3.2(\pm 1.7)$	$87.5 \pm 3.1(\pm 1.7)$
$80.9 \pm 2.8(\pm 1.7)$	$79.4 \pm 2.8(\pm 1.9)$	$89.9 \pm 3.1(\pm 1.7)$	$89.6 \pm 3.1(\pm 1.9)$	$94.1 \pm 3.3(\pm 1.5)$	$92.7 \pm 3.2(\pm 1.8)$	$95.7 \pm 3.3(\pm 1.7)$	$81.1 \pm 2.8(\pm 1.8)$
$78.6 \pm 2.8(\pm 1.6)$	$82.5 \pm 2.9(\pm 1.7)$	$93.9 \pm 3.3(\pm 1.7)$	$100.3 \pm 3.5(\pm 1.8)$	$101.6 \pm 3.6(\pm 1.7)$	$98.2 \pm 3.4(\pm 1.7)$	$93.5 \pm 3.3(\pm 1.6)$	$80.3 \pm 2.8(\pm 1.7)$

Table 2: Uniformity measurements at 500V, arranged according to Figure 3. Systematic (statistical) uncertainties are listed. Numbers are in channels between the signal and pedestal peaks.

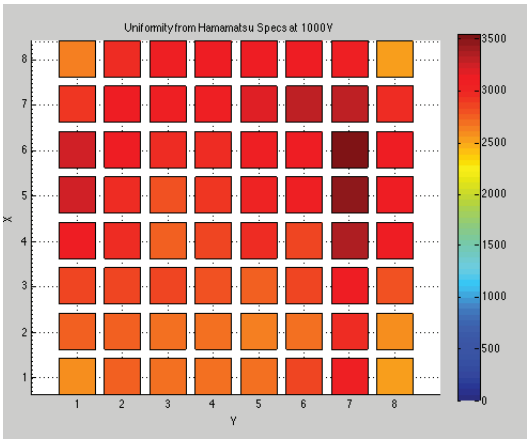

Figure 11: The uniformity specifications given by the manufacturer, scaled to match the 1000V measurement.

2443.9 ± 85.5(±30.8)	2668.6 ± 93.4(±31.0)	2573.2 ± 90.1(±29.0)	2866.1 ± 100.3(±32.0)	2880.9 ± 100.8(±31.3)	2951.2 ± 103.3(±31.5)	2723.4 ± 95.3(±29.4)	2642.8 ± 92.5(±29.9)
2745.5 ± 96.1(±32.4)	2941.0 ± 102.9(±34.4)	2827.9 ± 99.0(±33.7)	2910.9 ± 101.9(±35.0)	2886.9 ± 101.0(±34.0)	3256.4 ± 114.0(±35.1)	3286.8 ± 115.0(±34.0)	3008.1 ± 105.3(±33.7)
2649.3 ± 92.7(±32.2)	2800.0 ± 98.0(±34.2)	2798.9 ± 98.0(±34.8)	2838.9 ± 99.4(±34.7)	2851.7 ± 99.8(±34.2)	3054.7 ± 106.9(±35.8)	3244.8 ± 113.6(±35.4)	3151.6 ± 110.3(±35.6)
2645.9 ± 92.6(±32.5)	2654.2 ± 92.9(±32.6)	2815.6 ± 98.5(±33.0)	2867.6 ± 100.4(±33.1)	2946.3 ± 103.1(±34.0)	2992.6 ± 104.7(±34.7)	3265.4 ± 114.3(±35.2)	3208.3 ± 112.3(±36.1)
2658.2 ± 93.0(±32.2)	2639.4 ± 92.4(±32.2)	2752.0 ± 96.3(±32.3)	2991.7 ± 104.7(±34.6)	3072.6 ± 107.5(±35.3)	3175.9 ± 111.2(±37.0)	3266.8 ± 114.3(±36.2)	3294.6 ± 115.3(±35.6)
2713.8 ± 95.0(±32.2)	2694.0 ± 94.3(±32.2)	2773.6 ± 97.1(±33.3)	2912.4 ± 101.9(±34.8)	3149.4 ± 110.2(±37.4)	3167.6 ± 110.9(±37.3)	3415.3 ± 119.5(±30.4)	3253.6 ± 113.9(±35.6)
2931.6 ± 102.6(±34.7)	2917.1 ± 102.1(±33.1)	3105.2 ± 108.7(±35.3)	3334.4 ± 116.7(±37.5)	3328.1 ± 116.5(±36.1)	3503.3 ± 122.6(±27.2)	3548.0 ± 124.2(±18.2)	3196.0 ± 111.9(±36.0)
2913.6 ± 102.0(±36.7)	2867.1 ± 100.3(±33.6)	3075.9 ± 107.7(±35.2)	3415.9 ± 119.6(±29.1)	3391.5 ± 118.7(±32.0)	3393.1 ± 118.8(±30.3)	3453.8 ± 120.9(±26.7)	3175.0 ± 111.1(±36.9)

Table 3: Uniformity measurements at 1000V, arranged according to Figure 3. Systematic (statistical) uncertainties are listed. Numbers are in channels between the signal and pedestal peaks.

Tables 4-11 show the crosstalk strength at 500V and 850V, in fractions of signal strength. Where the signal and pedestal peaks were not possible to discern, an upper bound of two channels was imposed, as that is our maximum resolution.

$< .01 \pm .004$	$< .01 \pm .015$	$.014 \pm .004$
$< .01 \pm .027$		$.021 \pm .027$
$< .01 \pm .004$	$.024 \pm .015$	$.014 \pm .004$

Table 4: Crosstalk at 500V, centered around anode 14.

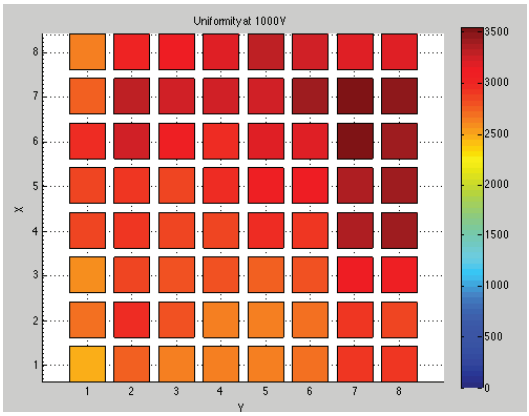

Figure 12: Uniformity at 1000V, signal strength given in channel number difference between the signal and pedestal peaks.

$< .01 \pm .004$	$.014 \pm .015$	$< .01 \pm .004$
$.011 \pm .027$		$< .01 \pm .027$
$.023 \pm .004$	$< .01 \pm .015$	$< .01 \pm .004$

Table 5: Crosstalk at 500V, centered around anode 46.

$.014 \pm .004$	$< .01 \pm .015$	$< .01 \pm .004$
$.027 \pm .027$		$< .01 \pm .027$
$< .01 \pm .004$	$< .01 \pm .015$	$< .01 \pm .004$

Table 6: Crosstalk at 500V, centered around anode 43.

$.012 \pm .004$	$< .01 \pm .015$	$< .01 \pm .004$
$.05 \pm .027$		$< .01 \pm .027$
$< .01 \pm .004$	$< .01 \pm .015$	$< .01 \pm .004$

Table 7: Crosstalk at 500V, centered around anode 11.

$< .01 \pm .004$	$.017 \pm .015$	$< .01 \pm .004$
$.012 \pm .027$		$.015 \pm .027$
$< .01 \pm .004$	$< .01 \pm .015$	$< .01 \pm .004$

Table 8: Crosstalk at 850V, centered around anode 14.

$< .01 \pm .004$	$.055 \pm .015$	$< .01 \pm .004$
$.014 \pm .027$		$.015 \pm .027$
$< .01 \pm .004$	$< .01 \pm .015$	$< .01 \pm .004$

Table 9: Crosstalk at 850V, centered around anode 46.

$.013 \pm .004$	$.017 \pm .015$	$< .01 \pm .004$
$.046 \pm .027$		$< .01 \pm .027$
$< .01 \pm .004$	$< .01 \pm .015$	$< .01 \pm .004$

Table 10: Crosstalk at 850V, centered around anode 43.

$< .01 \pm .004$	$.014 \pm .015$	$< .01 \pm .004$
$.043 \pm .027$		$< .01 \pm .027$
$< .01 \pm .004$	$< .01 \pm .015$	$< .01 \pm .004$

Table 11: Crosstalk at 850V, centered around anode 11.

All of our highest crosstalk measurements may be effected by a recurring phenomenon. Reference Figure 13. Remember that the measurements at anodes 7, 15, and 23 had to be taken in a separate run from the rest of the anodes, since the plug had to be moved. During the runs in this column, both when the fiber was

positioned at 14 and at 46, there appears to be some sort of background light turning on and off with the LED. The single red peak in the other two columns seems to indicate that light from the fiber four anodes below is not the source. A similar pattern occurs at the other pixels. If this is the case, than the second red peaks are the true pedestal for our crosstalk measurements, which would significantly reduce our higher crosstalk measurements.

6 Conclusions

Gain of each anode was determined to within 3.5%, at three separate voltages. The gain also appears to be in line with Hamamatsu's specifications. We also found that the maximum crosstalk was $\%5 \pm \%2.7$. However, with further testing, it is likely that this could be brought down to 2%.

7 Acknowledgements

This material is based upon work supported by the National Science Foundation under Grant No. PHY-1206053.

Thanks to my adviser, Dr Wouter Deconinck, lab partners Patrick Haurie and William Roh over the summer, and Yuxiang Zhou and Rakitha Beminiwattha especially for extensive help in understanding data acquisition and helping to design and troubleshoot these experiments..

8 Sources

Leo, William R. *Techniques for Nuclear and Particle Physics Experiments.* Berlin: Springer-Verlag,1994. Print.

Kyushima, Hiroyuki. Photomultiplier Tube with Dynode Array Having Venetian-blind Structure. Hamamatsu Photonics K.K., assignee. Patent US 5180943 A. 19 Jan. 1993. Print.